9 Superconductivity and Magnetism

D. Di Castro (till November 2004), D.G. Eshchenko, H. Keller, R. Khasanov,
S. Kohout, F. La Mattina (since March 2004), A. Maisuradze (since April 2004),
J. Roos, A. Shengelaya, S. Strässle (since December 2004)

visiting scientists: M. Eremin, V.A. Ivanshin, B. Kochelaev
Emeritus members: M. Mali, K.A. Müller (Honorarprofessor), T. Schneider (Titularprofessor)

in collaboration with:
ETH Zürich (K. Conder, J. Karpinski), Paul Scherrer Institute (K. Conder, E. Morenzoni), Max-Planck-Institute for Solid State Research Stuttgart (A. Bussmann-Holder), IBM Rüschlikon Research Laboratory (J.G. Bednorz), University of Birmingham (E.M. Forgan), University of Rome (A. Bianconi), Kazan State University (A. Dooglav, M.V. Eremin, V. Ivanshin, B.I. Kochelaev), University of Belgrade (I.M. Savić), University of Tokyo (K. Kishio, T. Sasagawa, H. Takagi).

Last year we continued our research activities on the magnetic and electronic properties of novel superconductors and related materials by means of a combination of different complementary experimental techniques, including muon-spin rotation (μSR), low-energy μSR, polarized neutron reflectometry, electron paramagnetic resonance (EPR), nuclear magnetic resonance (NMR), nuclear quadrupole resonance (NQR), as well as SQUID and torque magnetometry. The main goal of our investigation is to provide new information on the *macroscopic* and *microscopic* physical properties of high-temperature cuprate superconductors (HTS), other novel superconductors and related materials, which may help to understand the basic physics of these systems. In addition, we started a new project to investigate electric field effects on the electronic structure of Cr-doped strontium titanate by means of EPR in collaboration with the IBM Rüschlikon Laboratory.

9.1 Studies of isotope effects in novel superconductors

9.1.1 Polaron formation as origin of unconventional isotope effects in cuprate superconductors

High-temperature cuprate superconductors (HTS) are one of the most intensely studied systems due to the yet lacking understanding of the pairing mechanism. The antiferromagnetic properties of the undoped compounds are a consequence of the large Coulomb repulsion at the copper site. The energy scale given by it is the largest, and this has been taken as evidence that it must play a crucial role for the pairing mechanism. Consequently, effects stemming from the lattice have mostly been ignored, especially in view of the fact that the isotope effect on the superconducting transition temperature T_c almost vanishes at optimum doping (1; 2). The failure of BCS theory to account for many of the observed exotic properties has contributed to interpret the pairing mechanism in terms of a purely electronically driven one. However, various unexpected oxygen isotope (^{16}O/^{18}O) effects were reported (3)-(8) which are neither expected within the BCS mechanism nor within models based on strong correlations only. Since the Cu ion is one of the strongest Jahn-Teller systems (9), polaron formation can take place here and be the origin of unconventional isotope effects.

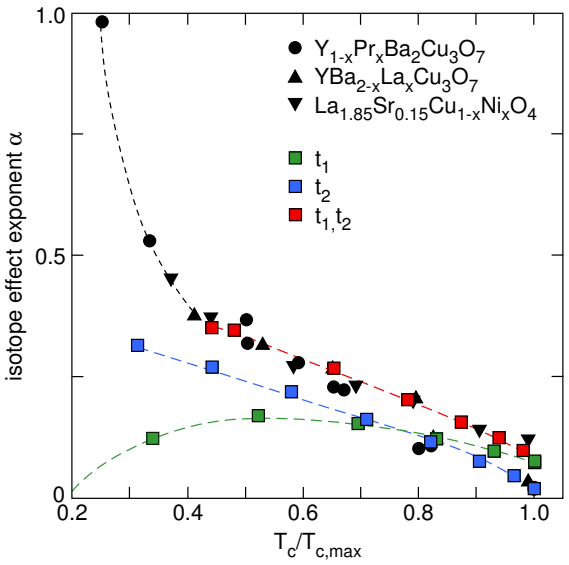

Figure 9.1:
Calculated isotope effect exponent α as a function of $T_c/T_{c,max}$ within the polaronic model [10] ($T_{c,max}$ is the maximum T_c for a given family of HTS). The red squares are calculated by renormalizing both hopping integrals t_1 and t_2 (see Fig. 9.2) through the polaronic coupling. The green squares are calculated by renormalizing t_1 only, whereas for the blue squares t_2 is renormalized, t_1 remains bare. The black symbols are experimental data points for various HTS taken from [7]. The dashed lines are a guide to the eye. The ratio of $t_2/t_1 = 0.3$.

In collaboration with A. Bussmann-Holder (Max-Planck-Institute for Solid State Research, Stuttgart) we investigated the origin of the isotope effects on the superconducting transition temperature and the magnetic penetration depth within polaron theory (10). For this purpose the well-known t-J Hamiltonian is extended to incorporate the hole induced charge channel and the important effects from the lattice. This results in a two-component Hamiltonian, where interactions between the charge channel (local hole plus induced lattice distortion) and the spin channel (antiferromagnetic fluctuations modified by lattice distortions) are explicitly included (10). It is found that the exponential squeezing of the second nearest neighbour hopping integral t_2 carries the correct isotope effect on the superconducting transition temperature T_c, as well as the one on the magnetic penetration depth λ. The average superconducting gap is predicted to have an isotope effect comparable to the one on the penetration depth λ. As an example, Fig. 9.1 shows the calculated isotope effect exponent $\alpha = -\mathrm{d}T_c/\mathrm{d}M$ (M is the oxygen mass) as a function $T_c/T_{c,max}$, together with experimental data (7) for comparison ($T_{c,max}$ is the maximum T_c for a particular family of HTS).

In order to clarify the symmetry of the coupling lattice distortion which causes these isotope effects, various renormalization procedures of the nearest (t_1) and the second nearest (t_2) neighbor hopping integrals were considered. It is evident from Fig. 9.1, that the isotope effect on T_c due to t_1 only, deviates strongly from experimental observations in the underdoped regime where it approaches zero. On the other hand, a renormalization of t_1 and t_2 with $t_2/t_1 = 0.3$ leads to values of $\alpha(T_c/T_{c,max})$ which are in excellent agreement with the experimental isotope effect data on T_c in the range $0.4 \leq T_c/T_{c,max} \leq 1$. However, at low doping the model does not describe the data satisfactory, which is probably due to fact that in a first step the same parameters are used in the model for all doping levels.

From this finding we conclude directly about the lattice distortion which governs the unconventional isotope effects. The half-breathing mode (Fig. 9.2, left panel), which shows anomalous softening (11), is dominated by t_1 and obviously exhibits the wrong isotope dependence. Since symmetry considerations also apply to the perpendicular direction of the half breathing mode, also the full breathing mode can be excluded. The crucial role of t_2 can only be taken into account by considering the Jahn-Teller active Q_2 type mode as the origin of the observed isotope effects (Fig. 9.2, right panel), consistent with the interpretation of earlier EPR results (12). Since the discovery of cuprate HTS (13) was motivated by the idea that Jahn-Teller polaron formation could be a new electron (hole) pairing mechanism, the present results support the original ideas.

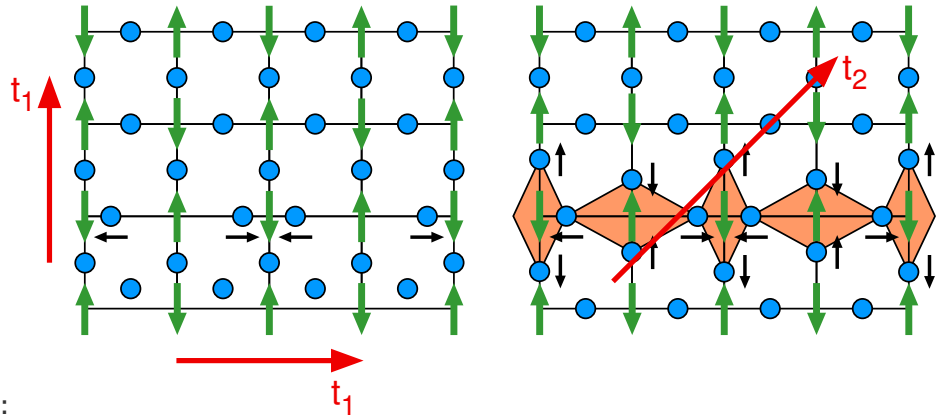

Figure 9.2:
The relevant ionic displacements which are either governed by t_1 only (left panel) or by t_2 only (right panel). Here only displacements in the CuO_2 plane are considered. The blue circles represent the oxygen ions, the green arrows are copper ions with the antiferromagnetic order. The black arrows in the left panel indicate the displacements for the LO half breathing phonon mode. Similarly a full breathing mode could be governed by t_1. The coloured rhombohedra show the displacements (black arrows) of the Q_2 type mode which is dominated by t_2.

[1] J.P. Franck, in **Physical Properties of High Temperature Superconductors IV** (ed. D.M Ginsberg) 189-293 (World Scientific, Singapore, 1994).

[2] D. Zech *et al.*, Nature **385**, 681 (1994).

[3] G.-M. Zhao, M.B. Hunt, H. Keller, and K.A. Müller, Nature **385**, 236 (1997).

[4] J. Hofer *et al.*, Phys. Rev. Lett. **84**, 4192 (2000).

[5] G.-M. Zhao, H. Keller, and K. Conder, J. Phys.: Condens. Matter **13**, R569 (2001).

[6] R. Khasanov *et al.*, Phys. Rev. Lett. **92**, 057602 (2004).

[7] R. Khasanov *et al.*, J. Phys.: Condens. Matter **16**, S4439 (2004).

[8] G.H. Gweon *et al.*, Nature **430**, 187 (2004).

[9] K.A. Müller, in **Magnetic Resonance and Relaxation** (ed. R. Blinc) 192-208 (North Holland Pbl. Inc., 1966).

[10] A. Bussmann-Holder and H. Keller, European Physical Journal B (2005), in press.

[11] M. Tachiki, M. Machida, and T. Egami, Phys. Rev. B **67**, 174506 (2003).

[12] B.I. Kochelaev *et al.*, Phys. Rev. Lett. **79,** 4274 (1997).

[13] J.G. Bednorz and K.A. Müller, Z. Phys.: Condens. Matter **64**, 189 (1986).

9.1.2 Oxygen Isotope effect on electronic phase separation in lightly doped $La_{2-x}Sr_xCuO_4$

Recently our EPR studies of lightly doped $La_{2-x}Sr_xCuO_4$ ($0 \leq x \leq 0.06$) revealed the presence of microscopic electronic phase separation of doped holes (1). However, the mechanism of the electronic phase separation in cuprates is still under debate. Up to now the main attention was paid to purely electronic and magnetic mechanisms, but the existence of phase separation within this approach is still controversial. Therefore, recently Kochelaev *et al.* (2) proposed an alternative mechanism. In the latter the electron-phonon coupling induces anisotropic interactions between the holes, resulting in the creation of extended nano-scale hole-rich regions. If phase separation is related with the electron-phonon coupling, one can expect an isotope effect on the formation of hole-rich and hole-poor

nanoscale regions in cuprates. We decided to check this possibility by studying the microscopic phase separation using EPR in lightly doped $La_{2-x}Sr_xCu_{0.98}Mn_{0.02}O_4$ with different oxygen isotopes (^{16}O and ^{18}O).
Figure 9.3 shows the temperature dependence of the narrow EPR line intensities for x = 0.02 samples with ^{16}O and ^{18}O oxygen isotopes. Previously, we showed that the appearance of this narrow line signals the formation of the hole-rich regions (1). Moreover, the formation energy Δ of these regions can be extracted from the temperature dependence of the signal intensity. One can see a clear difference between EPR signal intensities of the two isotope samples. The obtained results provide strong support for a phonon mechanism of phase separation in lightly doped $La_{2-x}Sr_xCuO_4$.

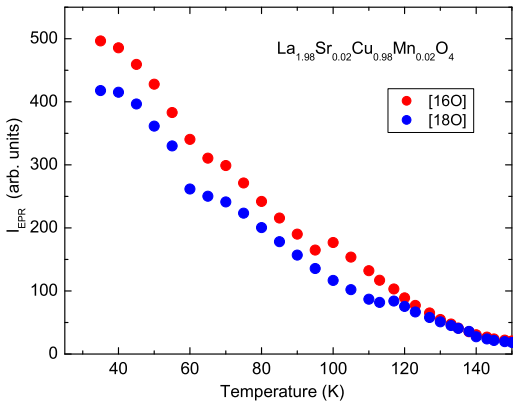

Figure 9.3:
Temperature dependence of the narrow EPR signal intensity for ^{16}O and ^{18}O samples of $La_{1.98}Sr_{0.02}Cu_{0.98}Mn_{0.02}O_4$.

[1] A. Shengelaya *et al.*, Phys. Rev. Lett. **93**, 017001 (2004).
[2] B. I. Kochelaev *et al.*, Mod. Phys. Lett. B **17**, 415 (2003).

9.2 Studies of pressure effects in novel superconductors

9.2.1 Pressure effect on the penetration depth in $YBa_2Cu_4O_8$

One way to explore the role of lattice vibrations in HTS is to perform isotope effect experiments. Previous studies (1)-(4) showed a substantial oxygen-isotope ($^{16}O/^{18}O$) effect on the in-plane penetration depth λ_{ab}, which indicates a non-adiabatic coupling of the electrons to phonon modes involving the movement of the isotope substituted atoms. An alternative way to explore lattice effects in HTS are pressure experiments. The squeezing of the crystal lattice by external hydrostatic or uniaxial pressure affects the lattice parameters, the phonon spectrum, and consequently the electron-lattice coupling. Surprisingly, the pressure effect (PE) on the magnetic field penetration depth has not attracted much attention yet.

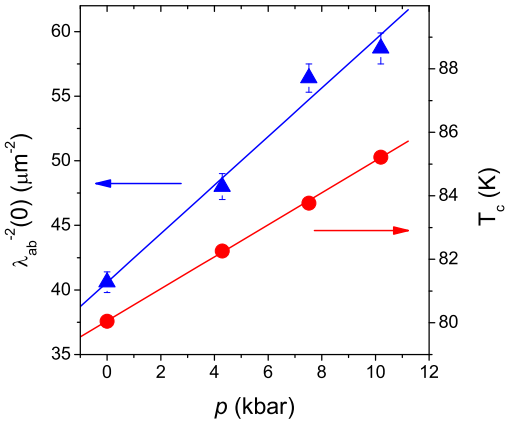

Figure 9.4:
Pressure dependence of the transition temperature T_c (circles) and the zero temperature in-plane magnetic penetration depth $\lambda_{ab}^{-2}(0)$ (triangles) in $YBa_2Cu_4O_8$.
The linear fits yield $dT_c/dp = 0.50(1)$ K/kbar and $d\lambda_{ab}^{-2}(0)/dp = 1.88(13)$ μm^{-2}/kbar.

Here we report the first observation of the pressure effect on the zero temperature in-plane magnetic field penetration depth $\lambda_{ab}(0)$ in a $YBa_2Cu_4O_8$ cuprate superconductor (5). A pronounced PE on both the transition temperature T_c and $\lambda_{ab}^{-2}(0)$ is observed which increases with increasing pressure (see Fig. 9.4). The pressure shift on $\lambda_{ab}^{-2}(0)$ is attributed to (i) the pressure induced charge carrier transfer from the chains to the planes and (ii) the decreasing of the in-plane charge carrier mass m_{ab}^*. At p =10.2 kbar we observed $\Delta\lambda_{ab}^{-2}(0)/\lambda_{ab}^{-2}(0) = 44(3)\%$ and $\Delta m_{ab}^*/m_{ab}^* = -32(3)\%$. Such a large effect on m_{ab}^* implies that lattice effects play an essential role in cuprate superconductors.

[1] G.-M. Zhao, M.B. Hunt, H. Keller, and K.A. Müller, Nature **385**, 236 (1997).

[2] J. Hofer *et al.*, Phys. Rev. Lett. **84**, 4192 (2000).

[3] R. Khasanov, *et al.*, J. Phys.: Condens. Matter **15**, L17 (2003).

[4] R. Khasanov *et al.*, Phys. Rev. Lett. **92**, 057602 (2004).

[5] R. Khasanov, J. Karpinski, and H. Keller, cond-mat/0405643.

9.2.2 Pressure effects on the transition temperature and the magnetic field penetration depth in the pyrochlore superconductor $RbOs_2O_6$

The temperature dependence of the magnetic field penetration depth λ reflects the quasiparticle density of states available for thermal excitations and therefore probes the superconducting gap structure. Observation of a high pressure effect on T_c is a good indication that higher values of T_c in similar compounds may be obtained by "chemical" pressure (by exchanging the appropriate ion with its chemical equivalent having a different ion size). It is not widely appreciated, however, that the pressure dependence of T_c, like the isotope dependence, contains valuable information on the superconducting mechanism itself.

We performed magnetization measurements in the recently discovered superconductor $RbOs_2O_6$ under hydrostatic pressure (1). A pronounced and *positive* pressure effect on T_c with $\mathrm{d}T_c/\mathrm{d}p = 0.090(1)$ K/kbar was observed (see Fig. 9.5), in contrast to the negative pressure shift generally detected in conventional superconductors. This finding was explained within the framework of BCS theory under the assumption that the electron-phonon coupling constant λ_{el-ph} increases with pressure. The absence (within the experimental uncertainties) of a pressure effect on λ suggests that $RbOs_2O_6$ is an adiabatic BCS–type superconductor.

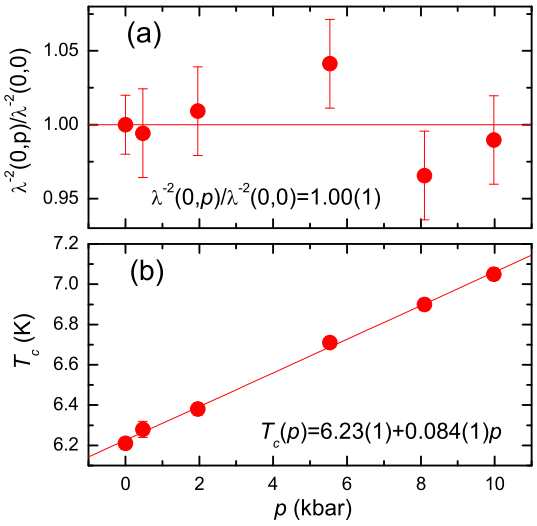

Figure 9.5:
The pressure dependence of $\lambda^{-2}(0)(p)/\lambda^{-2}(0)(p=0)$ (a) and T_c (b) in $RbOs_2O_6$. The solid lines are fits with parameters shown in the figure.

[1] R. Khasanov *et al.* Phys. Rev. Lett. **93**, 157004 (2004).

9.3 Spectroscopic studies of novel superconductors

9.3.1 NMR/NQR investigations of YBCO compounds

We continued our collaboration with the research group of A.V. Dooglav and M. Eremin at the State University of Kazan (Russia). The investigation of the plane ^{63,65}Cu spin-lattice relaxation in superconducting $\mathrm{YBa_2Cu_4O_8}$ at mK temperatures is being completed with a study of the related Ca doped compounds $\mathrm{Y_{1-x}Ba_{2-y}Ca_{x+y}Cu_4O_8(x+y=0.02, 0.05, 0.1)}$ down to 1.5K.

In the superconducting phase of $\mathrm{YBa_2Cu_4O_8}$ the magnetic contribution to the Cu spin-lattice relaxation due to spin fluctuations diminishes because of the superconducting gap (1). At very low temperature this reduced relaxation progressively changes its character from magnetic towards quadrupolar with an unexpectedly large increase in rate below 1K (2). In contrast, $\mathrm{Y_{1-x}Ba_{2-y}Ca_{x+y}Cu_4O_8}$ shows a similar feature shifted to higher temperature regions. The location of this feature on the temperature scale strongly depends on the details of the distribution (x, y) of Ca onto Y or Ba sites (3). With increasing Ca substitution this feature seems to move more near to the superconducting transition temperature. Consequently, spin-lattice relaxation of magnetic character due to spin fluctuations regains its dominance, masking progressively the quadrupolar relaxation contribution.

In our NQR search in cuprates for effects of charge inhomogeneities that seem to exist as self organized objects and are possibly related to the appearance of the pseudo-gap, we recently performed ^{175}Lu NQR measurements on $YBa_2Cu_3O_7$ single crystals. The site symmetry of Lu causes anti-ferromagnetic Cu spin fluctuations to cancel. NQR at this site is therefore exclusively sensitive to charge effects. However, due to the very large nuclear quadruple moment of ^{175}Lu charge fluctuations lead to an extreme shortening of the Lu spin-lattice relaxation time, rendering Lu NQR signals practically undetectable within the experimentally available temperature range. Since high quality powder samples of $LaBa_2Cu_3O_7$ have recently been synthesized successfully by K. Conder and E. Pomjakushina (Paul Scherrer Institute, PSI and ETH Zürich) we were able to resume work on this topic by starting ^{139}La NMR/NQR investigations of $LaBa_2Cu_3O_7$. The nuclear quadrupole moment of ^{139}La is approximately 30 times smaller than the one of ^{175}Lu thus preventing an unfavourable excessive increase of spin-lattice relaxation as observed in the case of Lu. Our preliminary results show an unusual behavior of ^{139}La spin-lattice and spin-spin relaxation in the normal conducting phase of $LaBa_2Cu_3O_7$ below 300K possibly related to charge inhomogeneity effects.

In recent theoretical investigations the appearance of a new phase in cuprates characterized by so-called orbital currents in the CuO_2 planes was predicted (see e.g. (4)). It was suggested to check for their existence by ^{89}Y NMR in the compound $Y_2Ba_4Cu_7O_{15}$, where the Y site is neighboured by unequally doped CuO_2-planes (5). To perform this task we started a study of the temperature dependence of various Y NMR parameters in this compound in order to detect a static or dynamic response to possible orbital currents. We measured the temperature dependence of the Y NMR line shift and line width in normal conducting $Y_2Ba_4Cu_7O_{15}$ and were able to determine within errors an upper limit for a static magnetic field caused by an averaged response to possible orbital currents, which is far below predicted values.

[1] M. Bankay *et al.*, Phys. Rev. B **50**, 6416 (1994).

[2] M. Mali *et al.*, J. Supercond. **15**, 511 (2002).

[3] M. Mali, J. Roos, and D. Brinkmann, Phys. Rev. B **53**, 3550 (1996).

[4] D.A. Ivanov *et al.*, Phys. Rev. Lett. **84**, 3958 (2000).

[5] P.A. Lee and G. Sha, Solid State Commun. **126**, 71 (2003).

Table 9.1: **Summary of the μSR results obtained for $RbOs_2O_6$ ($\mu_0 H$: external magnetic field, T_c: superconducting transition temperature, Δ_0: zero-temperature energy gap, $\lambda(0)$: zero-temperature magnetic penetration depth).**

$\mu_0 H$ (T)	T_c (K)	Δ_0 (meV)	$\lambda(0)$ (nm)
0.1	6.24(3)	0.97(4)	252-256
0.5	6.00(4)	0.87(3)	268-288
1	5.59(2)	0.80(3)	254-295
2.5	4.36(2)	0.58(5)	232-325

9.3.2 Study of the magnetic penetration depth in $RbOs_2O_6$

Since the discovery of superconductivity in pyrochlore related oxides there is no agreement about the nature of superconducting pairing mechanism in these compounds. Investigations of specific heat (1), pressure effects on the magnetic field penetration depth (2) and NMR in $RbOs_2O_6$ (3), as well as band structure calculations of KOs_2O_6 (4) point to a conventional type of superconductivity. In contrast, measurements of the second critical field H_{c2} (5), μSR (6; 7), and specific heat (5) suggest an unconventional type of paring in KOs_2O_6 and $RbOs_2O_6$.

The results of our μSR study of the temperature dependent magnetic penetration depth $\lambda(T)$ in $RbOs_2O_6$ (see Ref. (8) for details) are summarized in Table 9.1 and yield the following findings:

- The absolute value of λ at zero temperature is in the range of 250 nm to 300 nm.
- For temperatures down to 30 mK the temperature dependence of λ is consistent with what is expected for a weak–coupled s–wave BCS superconductor (see Fig. 9.6).
- The shape of $\lambda(T)$ is almost independent of the magnetic field.
- The value of the zero-temperature superconducting gap decreases with increasing magnetic field (decreasing of T_c). The ratio $2\Delta_0/k_B T_c$ was found to be in the range of 3.09–3.60 close to the weak-coupling BCS value 3.52.

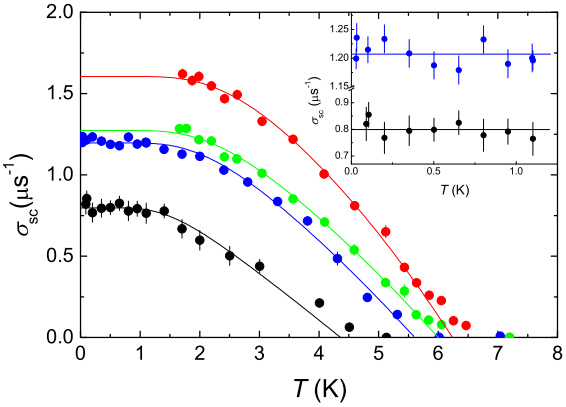

Figure 9.6:
Temperature dependence of the superconducting part of the μSR depolarization rate $\sigma_{sc} \propto \lambda^{-2}$ of $RbOs_2O_6$, measured in fields (field-cooled) of 0.1 T, 0.5 T, 1 T, and 2.5 T (from the top to the bottom). The inset shows the low-temperature region between 0 K and 1.25 K. The constant (within error bars) $\sigma_{sc}(T) \propto \lambda^{-2}$ suggests that $RbOs_2O_6$ is a weak-coupled BCS superconductor. Solid lines represent fits with the expression for the weak-coupling BCS model given in [8].

- The μSR measurements show that at low temperatures the magnetic penetration depth λ is almost (within an accuracy of 10%) field independent, in agreement with what is expected for a superconductor with an isotropic energy gap.

These facts suggest that $RbOs_2O_6$ is *a weak-coupled BCS superconductor with isotropic energy gap*.

[1] M. Brühwiler *et al.*, Phys. Rev. B **70**, 020503(R) (2004).
[2] R. Khasanov *et al.*, Phys. Rev. Lett. **93**, 157004 (2004).
[3] K. Magishi *et al.*, cond-mat/0409169.
[4] R. Saniz *et al.*, Phys. Rev. B **70**, 100505 (2004).
[5] Z. Hiroi *et al.*, J. Phys. Soc. Jpn **73**, 1651 (2004).
[6] R. Kadono, J.Phys.: Condens. Matter **16**, S4421 (2004).
[7] A. Koda *et al.*, cond-mat/0402400.
[8] R. Khasanov *et al.*, cond-mat/0411674.

9.3.3 Tri-layer $YBa_2Cu_3O_7/PrBa_2Cu_3O_7/YBa_2Cu_3O_7$ studies by means of low-energy μSR and polarized-neutron reflectometry

One of the most remarkable unconventional effects in HTS is the recently observed giant proximity effect (see e.g. (1) and references therein). A supercurrent in Josephson junctions was found to run through relatively thick non-superconducting barriers. This contradicts conventional theories which predict exponential suppression of supercurrents with increasing barrier thickness because of the short coherence length of HTS's.
Recent advances in fabrication and characterization of multilayers based on perovskite oxides have opened a new avenue in the investigation of various physical phenomena in superconductor/ferromagnet and superconductor/insulator heterostructures needed in the fabrication of Josephson and proximity effect junctions. Last year we started low-energy μSR measurements in a $33\,\mathrm{nm}/50\,\mathrm{nm}/115$ nm $YBa_2Cu_3O_7/PrBa_2Cu_3O_7/\ YBa_2Cu_3O_7$ structure grown at the University of Geneva. The measurements in a weak magnetic field $\mathrm{B_{ext}}$ = 19.54 mT applied parallel to the surface of the tri-layer sample at a temperature of 5K are presented in Fig. 9.7. Implantation energies of incoming muons were tuned to stop most of the muons in the appropriate layer (3 keV/12.5 keV/30 keV).

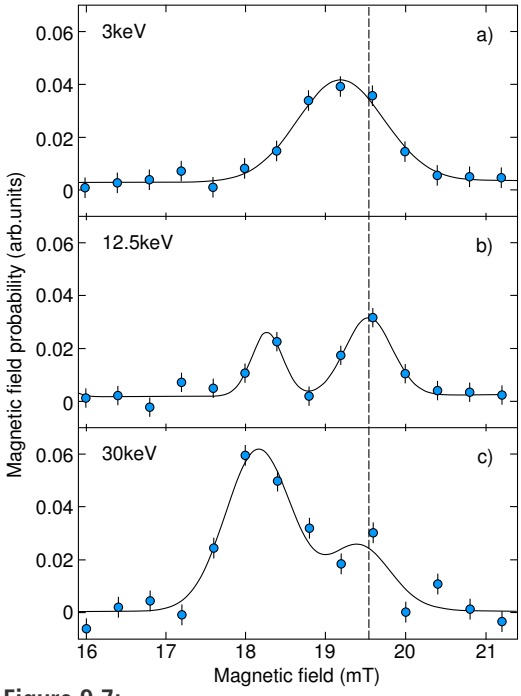

Figure 9.7:
Magnetic field distributions measured at T=5K in external magnetic field Bext=19.54mT (dashed line) in: a) first $YBa_2Cu_3O_7$ layer; b) intermediate $PrBa_2Cu_3O_7$ layer; c) second $YBa_2Cu_3O_7$ layer.

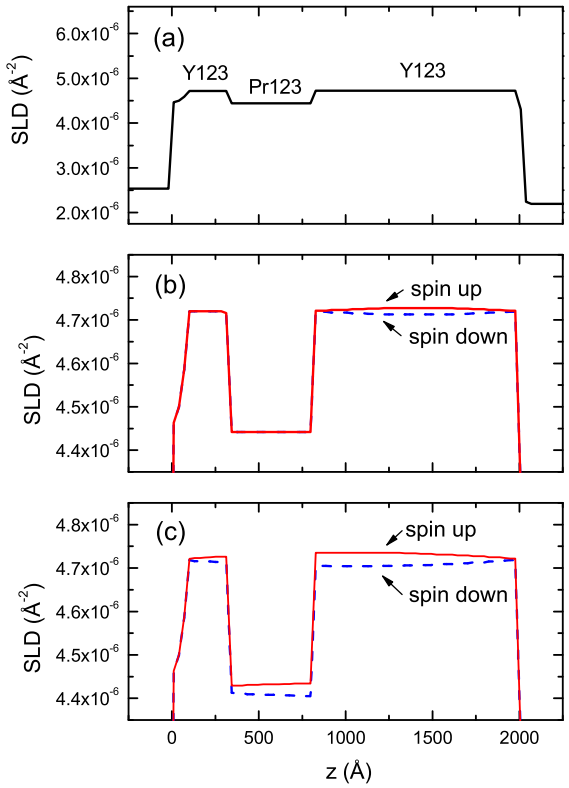

Figure 9.8:
The SLD profiles in the $YBa_2Cu_3O_7/PrBa_2Cu_3O_7/YBa_2Cu_3O_7$ tri-layer sample in the normal state (a) and in the superconducting state (b and c). The solid and dashed lines in (b) and (c) denote the SLD profiles for spin-up and spin-down neutrons, respectively.

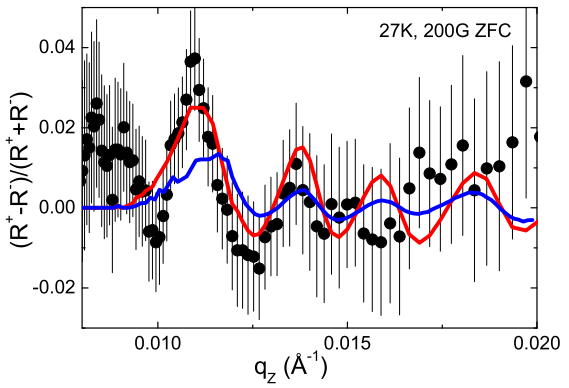

Figure 9.9:
$(R^+ - R^-)/(R^+ + R^-)$ vs. q_z ($T = 27$ K, $H = 200$ G zero-field cooled) for the $YBa_2Cu_3O_7/PrBa_2Cu_3O_7/YBa_2Cu_3O_7$ tri-layer sample. The blue and red lines are calculated for the models presented in Figs. 9.8(b) and (c), respectively.

One can see that the magnetic field is screened not only inside both superconducting layers, but there is a pronounced peak of the internal field distribution function well below the applied magnetic field inside the intermediate antiferromagnetic layer. To check if this behavior is due to the superconductor/antiferromagnet interface we are planning experiments in $PrBa_2Cu_3O_7$ thin films and $YBa_2Cu_3O_7/PrBa_2Cu_3O_7/YBa_2Cu_3O_7$ tri-layers with different thicknesses of individual layers.

In contrast to local techniques used so far in the study of the giant proximity effect, polarized-neutron reflectivity is a bulk method that can help to clarify whether giant proximity, pinholes and/or microshorts are responsible for the observed effects.

Here we report first preliminary studies of the giant proximity effect by means of the polarized neutron reflectivity technique. The tri-layer sample consists of $YBa_2Cu_3O_7/PrBa_2Cu_3O_7/YBa_2Cu_3O_7$ layers with relative thicknesses 33nm/50nm/115nm. First preliminary measurements of neutron scattering lengths density (SLD) profiles of the trilayer sample are shown in Fig. 9.8. In the normal state the SLD profile is determined by neutrons scattered by the nuclei, and it is expected to be equal for spin-up and spin-down polarized neutrons (Fig. 9.8(a)). In the superconducting state the magnetic field is expelled from the superconducting volume of the sample. Thus, in addition to pure nuclear scattering, magnetic scattering occurs and causes the difference in SLD profiles for spin-up and spin-down neutrons. Two simple models were tested. In the first one (see Fig. 9.8(b)), it was assumed that the magnetic field is screened only within the two superconducting $YBa_2Cu_3O_7$ layers, while in the antiferromagnetic $PrBa_2Cu_3O_7$ layer it is equal to the external field. In the second model the whole structure was assumed to be superconducting (see Fig. 9.8(c)). To remove the nuclear contribution in the reflectivity spectra $R(q_z)$, the ratio $(R^+ - R^-)/(R^+ + R^-)$ was determined

as shown in Fig. 9.9. Here q_z denotes the neutron wave vector, and the indexes $+$ and $-$ stay for spin-up and spin-down, respectively. The comparison of the experimental data with the curves calculated for the models presented in Figs. 9.8(b) and (c) leads to the conclusion that most probably the superconducting $YBa_2Cu_3O_7$ layers are coupled through the antiferromagnetic $PrBa_2Cu_3O_7$ layer. This statement is in agreement with our low-energy μSR measurements performed on the very same sample.

[1] I. Bozovic *et al.*, Phys. Rev. Lett. **93**, 157002 (2004).

9.4 Electric field effects in perovskites

9.4.1 Insulator-to-metal transition and resistive memory effect in perovskites induced by electric field

There has been an increased interest in investigating various sorts of *Random Access Memories* that retain stored information after removing the electrical power from the device, i.e., nonvolatile memory. Simpler memory cells presently under intense investigation are using the resistance change of a medium by current or voltage pulses, an effect observed in a large variety of extremely diverse materials.
Starting a collaboration with IBM Rüschlikon Laboratory, we are currently investigating the resistive switching effect that has been found in thin films of perovskites like (Ba,Sr)TiO_3, $SrZrO_3$, $SrTiO_3$ (1).These materials exhibit a charge-induced insulator-to-metal transition with a resistive memory effect. Exposed to an electrical field, the resistance of the doped perovskite is reduced by several orders of magnitude and a conductor is obtained, which is a prerequisite for the memory switching. Consecutive electrical current pulses of opposite polarity switch the resistance of the perovskite reversibly between a high-resistance and a low-resistance state (see Fig. 9.10). These two different states persist after removal of the applied electrical bias with a retention time of up to several years. Single crystals of Cr-doped $SrTiO_3$ (2) with the same memory behavior are used as a model system for this class of materials to study the drastic resistivity changes in the bulk under applied electrical field , the switching between memory levels and to clarify the role of defects with different valencies.

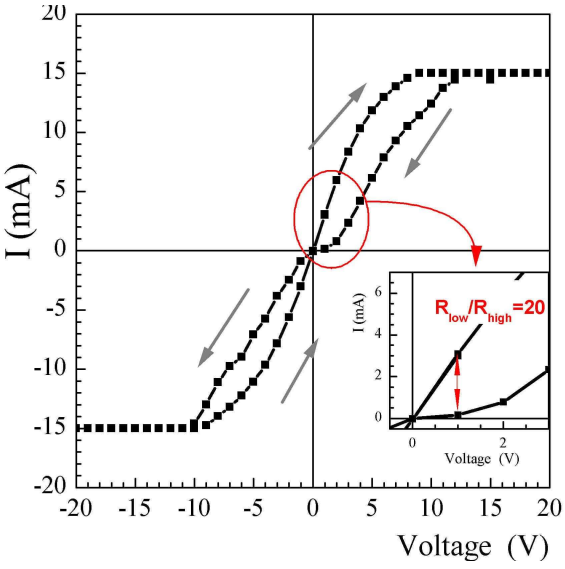

Figure 9.10:
Current-Voltage characteristic (I-V) on Cr-doped $SrTiO_3$ single crystal. Once the insulator-to-metal transition is reached, one finds a hysteresis behavior in the I-V curve.

Changes of the electronic state of the Cr dopant are detected by X-ray absorption spectroscopy on crystals during electrical stressing where it is possible to detect the transformation of Cr^{3+} to Cr^{5+} in a volume close to the metal electrode (anode). It is clear that in this material the Cr ion and its different valence states (3) play a crucial role. Therefore, we decided to study these materials using EPR. In a first step two different $SrTiO_3$:Cr single crystals were measured: annealed in a reducing atmosphere (Ar/H_2) and in an oxidizing atmosphere. It was found that in the oxidized crystals the

majority of Cr ions are in the 5+ valence state. A significant amount of Cr is still seen in the trivalent state. On the other hand, in reduced crystals only Cr^{3+} centers were observed with no evidence of the presence of Cr^{5+}.

In order to study the influences of Cr on the electronic structure of $SrTiO_3$ we performed dielectric and optical absorption measurements. By varying the defect (dopant) concentration (from 0.1 mol% to 0.2 mol%) in single crystals the dielectric properties are modified. Dielectric properties change even more drastically with the Cr valence state. Another evidence of the Cr influence on the electronic structure is the changes of the energy gap between the valence and conduction bands detected by optical absorption in the UV-visible range (from 3.2eV in the undoped samples to 2.5eV in samples with 0.2 mol% of Cr).

[1] A. Beck *et al.*, Appl. Phys. Lett. **77**, 139 (2000)
[2] Y. Watanabe *et al.*, Appl. Phys. Lett. **78**, 3738 (2001)
[3] K.A. Müller *et al.*, Solid State Commun. **85**, 381 (1993)

9.5 New developments in instrumentation

9.5.1 Novel design of piezoresistive torque sensors

Torque magnetometry is a powerful measurement technique, employed in studies of anisotropic and hysteretic magnetic systems. We have been using it successfully for investigations of cuprate superconductors for a decade (1)-(3). During this time, we have also improved this technique several times (4)-(6). The piezoresistive torque detection exploits the resistance change of doped silicon under stress. Since the application of a torque on a suitably formed sensor induces stress in the structure, this allows for an easily detectable and very sensitive determination of the applied torque. Recently we have considered and calculated sensor shapes differing from the initially used cantilever design adopted from atomic force microscopy tips. Our novel design is more flexible and allows expendability compared to those tips. The new square shape of torque sensors allows for the implementation of additional functionality. In Fig. 9.11 a version is shown with the integrated calibration loop and a diode for temperature measurement at the sample position. The fabrication of a sensor, sensitive along two directions, is possible, when all four legs are equipped with piezoresistive paths. Moreover, the sensitivity and robustness can be influenced by modifying the length of the legs. Longer legs result in higher sensitivity, but also cause the sensor to become more fragile and likely to break when a sample is mounted.

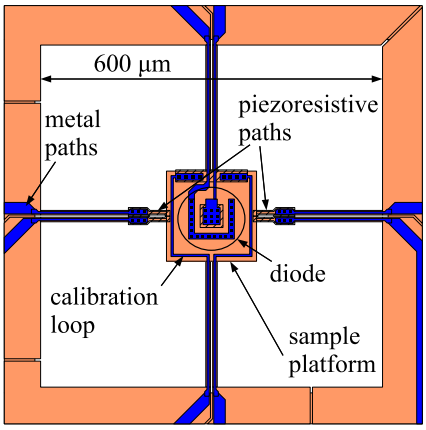

Figure 9.11:
New square shape design with calibration loop and diode for temperature measurement. Piezoresistive paths (hatched areas) are situated on the left and right legs, close to the sample platform. The sensor is embedded in a large $4 \times 5\,\mathrm{mm}^2$ chip. The metallic paths (colored blue) provide the electrical connections.

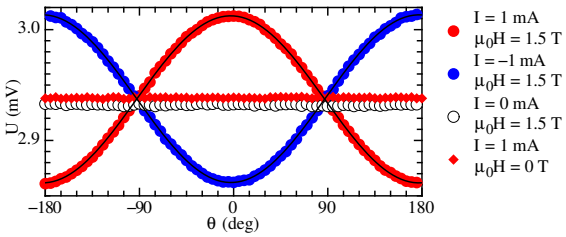

Figure 9.12:
Angle dependent measurements with the new high sensitivity torque sensor shown in Fig. 9.11 in various magnetic field strengths H and calibration loop currents I. Solid lines represent simple cosine-fits. The amplitude of the cosine signal amounts to $2.85 \times 10^{-11}\,\mathrm{Nm}$ in terms of absolute torque.

A metallic loop incorporated on the sample platform allows the induction of a small magnetic moment. Angle dependent measurements in fixed magnetic fields then allow for the relation of the measured voltage to absolute torque magnitudes (example is shown in Fig. 9.12).

[1] D. Zech *et al.*, Phys. Rev. B **54**, 12535 (1996).
[2] M. Willemin *et al.*, Phys. Rev. Lett. **81**, 4236 (1998).
[3] J. Hofer *et al.*, Phys. Rev. Lett. **84**, 4192 (2000).
[4] C. Rossel *et al.*, J. Appl. Phys. **79**, 8166 (1996).
[5] M. Willemin *et al.*, J. Appl. Phys. **83**, 1163 (1998).
[6] C. Rossel *et al.*, Rev. Sci. Instrum. **69**, 3203 (1998).

9.5.2 Automation of the torque measurement setup

Modern scientific work increasingly requires extensive studies in order to detect systematic effects across a large variety of samples and measurement conditions. Measurement automation greatly facilitates such time consuming experiments, but is mostly available only in commercial apparatuses. The control software shipped with such systems is usually created and improved over years by specialized software development teams. Such costly development is seldom within the possibilities of research laboratories, which is why the computer programs used to control custom built experiments are often comparably simple and allow only restricted automation.
A relatively simple program architecture allowed us to create a highly versatile control software system for our custom torque magnetometer (1). Our approach comprises the use of individual programs running in parallel with appropriate means of communication between them. This makes possible the use of an additional program to control the whole system. In our current implementation, this additional program works through a previously created sequence of commands. The nearly arbitrary complexity permitted for such sequences enables us to have the system conduct long measurement series automatically. The basic structure is very general which makes both the application to other instruments and the expansion to more complexity very easy. Currently, we are working on its adaptation to an EPR spectrometer. Since the system is programmed using LabVIEW, an easy to learn graphical programming language, its modification and extension is further facilitated. Thus, the automatic adaptation of experimental parameters based on measurement results during the measurement itself might also be made possible.

[1] S. Kohout, J. Roos, and H. Keller, submitted for publication.